



# Engineering a uniaxial substrate-stretching device for simultaneous electrophysiological measurements and imaging of strained peripheral neurons

Fabio Bianchi<sup>a</sup>, Julian H. George<sup>a</sup>, Majid Malboubi<sup>b,c</sup>, Antoine Jerusalem<sup>b</sup>, Mark S. Thompson<sup>a</sup>, Hua Ye<sup>a,\*</sup>

<sup>a</sup>Institute of Biomedical Engineering, Dept. of Engineering Science, University of Oxford, Oxford OX3 7DQ, UK

<sup>b</sup>Department of Engineering Science, University of Oxford, Oxford OX1 3PJ, UK

<sup>c</sup>Department of Mechanical Engineering, The University of Birmingham, Birmingham B15 2TT, UK

## ARTICLE INFO

### Article history:

Received 6 October 2018

Revised 17 February 2019

Accepted 25 February 2019

### Keywords:

Peripheral nerve

Uniaxial strain

Nerve damage

Patch clamping

Calcium imaging

## ABSTRACT

Peripheral nerves are continuously subjected to mechanical strain during everyday movements, but excessive stretch can lead to damage and neuronal cell functionality can also be impaired. To better understand cellular processes triggered by stretch, it is necessary to develop *in vitro* experimental methods that allow multiple concurrent measurements and replicate *in vivo* mechanical conditions. Current commercially available cell stretching devices do not allow flexible experimental design, restricting the range of possible multi-physics measurements.

Here, we describe and characterise a custom-built uniaxial substrate-straining device, with which neurons cultured on aligned patterned surfaces (50  $\mu\text{m}$  wide grooves) can be strained up to 70% and simultaneously imaged with widefield and confocal imaging (up to 100x magnification). Furthermore, direct and indirect electrophysiological measurements by patch clamping and calcium imaging can be made during strain application. We characterise the strain applied to cells cultured in deformable wells by using finite element method simulations and experimental data, showing local surface strains of up to 60% with applied strains of up to 25%. We also show how patterned substrates do not alter the mechanical properties of the system compared to unpatterned surfaces whilst still inducing a homogeneous cell response to strain.

The characterisation of this device will be useful for research into investigating the effect of whole-cell mechanical stretch on neurons at both single cell and network scales, with applications found in peripheral neuropathy modelling and in platforms for preventive and regenerative studies.

© 2019 The Author(s). Published by Elsevier Ltd on behalf of IPEM.

This is an open access article under the CC BY license. (<http://creativecommons.org/licenses/by/4.0/>)

## 1. Introduction

The peripheral nervous system (PNS) is tolerant to continuous mechanical stresses during ordinary movements, but supraphysiological extension can lead to injury. Nerve damage can be a result of traumatic events, a by-product of surgery, or due to chronic conditions. Erbs palsy, for example, is caused by excessive stretching of infant heads and arms during labour inducing loss of sensation and abnormal motor function in 0.1% of births in the US [1].

Neuron deformation has been shown to alter ion channel functionality [2], depress neural network activity [3], and cause cytoskeletal damage and collapse [4], implicating mechanotrans-

duction in neural damage. To better understand the mechanisms involved, cell-scale *in vitro* models reproducing the mechanical environment of the PNS are required. *Ex vivo* animal tissue does not allow for the investigation of neural cell response in isolation, so *in vitro* experimental devices have been designed to investigate a wide variety of biological responses to mechanical stimuli, but none specifically for PNS modelling (see review by Kamble et al. [5]).

Existing devices can be classified by actuation mechanism. Electromagnetic actuation, where substrate deformation is directly induced by a motor, includes uniaxial [6,7] and biaxial [8] systems. Air-pressure pulse actuated systems provide equibiaxial strain, and deliver highly uniform strain fields to deformed substrates [9]. Fluid flow actuated devices are used to investigate shear force as a mechanical stimulus [10]. Other actuation mechanisms

\* Corresponding author.

E-mail address: [hua.ye@eng.ox.ac.uk](mailto:hua.ye@eng.ox.ac.uk) (H. Ye).

such as piezoelectric [11] and thermal [12] have been used in cell-stretching devices, but can deliver only limited magnitudes of strain. The PNS is a highly anisotropic axially aligned structure, pointing to direct uniaxial electromagnetic actuation as the most suitable actuation method.

PNS conduction disruption caused by nerve straining is poorly understood, partly due to the lack of *in vitro* models to study the direct effect of strain on nerve electrophysiological function. Previous studies mostly separate mechanical stimulus from the electrical recording, introducing a time delay in the effects observed [2,3]. Flexible multi-electrode array (MEA) systems can be used to quantify the effect of strain and shear on *in vitro* and *in vivo* neural electrophysiology [13–15], but do not allow for confocal imaging and do not provide single-cell data. A substrate-towing device used to produce stretch-grown dorsal root ganglion neurons has previously been combined with patch clamping, calcium imaging, and confocal imaging [16], but was aimed at studying stretch-growth rather than damage. Indirect electrophysiology measurements by calcium flux imaging have been carried out simultaneously with applied strain [17], but do not probe the response of individual cells. Most non-electromagnetically actuated systems require bulky equipment, complex disassembling for transport, and do not give users the flexibility to perform multi-physics experimental recordings. Commercially available systems such as FlexCell FX-5000 (USA) [18], Strex STB-10 (Japan) [19] and ALA scientific MEASSURE (USA) offer limited flexibility of system design and experimental parameters, and are therefore unsuited for integration with multi-physics measurement setups.

At the cellular level, cell bodies within nerve roots and axonal projections through endoneurial channels experience deformation during limb movement [20,21]. Cell alignment is therefore a key parameter to replicate the *in vivo* mechanical environment of peripheral nerves. *In vitro*, neurons align to substrate features at the micro- and nano-scale [22]. In existing straining devices, growth templates applied before seeding and removed before strain application have been used [7,23]. This aligns cells prior to deformation, but does not provide structural support similar to *in vivo* conditions. Furthermore, cells can be damaged when the growth templates are removed. Alternatively, neurons have been aligned in enclosed microfluidic channels and exposed to mechanical stimuli [24], making cells inaccessible and electrophysiology more challenging.

Here, we introduce the first reported example of a displacement controlled substrate-stretching device with the aim of recording high-resolution wide-field and confocal microscopy, single-cell patch clamping, and indirect network electrophysiology measurements during the application of uniaxial strain to cultured neurons. The use of manufactured deformable cell culture wells with aligned grooved substrates replicates the *in vivo* morphological environment of peripheral nerves. We present a compact system, allowing easy transport and setup, simultaneous direct (patch clamp) and indirect (calcium imaging) electrophysiological measurements during uniaxial strain. We characterise the substrate deformation by recording experimental measurements and performing finite element method simulations, precisely calibrating the use of this device for neuron deformation experiments.

## 2. Materials and methods

### 2.1. Device design and manufacturing

The cell stretching device was designed in four parts: the motor (Zaber Technologies NA08B30-T4 linear actuator, X-MCB1 controller), the sample holder, the deformable well and the microscope stage adaptor (Fig. 1). Microscope stage adaptors were designed to fit Nikon and Zeiss microscope stages, and CNC-

machined from black anodised aluminium to minimise imaging glare. The sample holder was manufactured by stereolithographic 3D printing (Form 2 printer, FormLabs) using clear photocurable resin, with a layer height of 25  $\mu\text{m}$ . Following printing, components were cured in 90% ethanol for 30 min then left to air-dry for 2 h.

### 2.2. Design and manufacturing of deformable wells

The deformable wells were manufactured from polydimethylsiloxane (PDMS, Dow Corning) cast in a 3D printed mould manufactured by stereolithographic 3D printing (Form 2 printer, FormLabs) using clear photocurable resin. The wells measured  $45 \times 20 \times 3$  mm, with a  $10 \times 6.5$  mm rectangular feature at the centre. PDMS was mixed at 1:10 ratio between curing and base agents, vacuum degassed, injected into the mould using a syringe at 2.5 ml per mould and cured at 60 °C for 4 h. Ultra-thin 50 and 100  $\mu\text{m}$  ( $\pm 5\%$ ) PDMS films (Elastosil, Silex Ltd) were bonded to the bottom of the well using a thin layer of PDMS and cured for 1 h at 60 °C to create watertight wells with thin transparent bases. To simulate neural alignment present in peripheral nerves, PDMS films with aligned microgrooves were manufactured by casting a thin layer of PDMS on a microgroove template (vinyl record 'Bird Sounds in Up Close' by Victor C. Lewis, with consistent groove width and depth) and cured for 1 h at 60 °C. Grooved film thickness was measured using a manual micrometer to be  $130 \pm 30$   $\mu\text{m}$  ( $n = 5$  independently cast films).

### 2.3. Scanning Electron Microscope (SEM) Imaging

Grooved PDMS surfaces were placed on adhesive carbon discs and imaged using a Hitachi TM3030plus tabletop SEM, under high vacuum and with a 15 kV acceleration voltage.

### 2.4. Finite element method simulations

Finite element simulations were carried out using Simulation Mechanical (Autodesk Inc.). The model was simplified to include only the clamps, deformable well and grooved or smooth substrate. Non-slip conditions were assumed between clamps and well and between the well and substrate. The stationary clamp was constrained in all directions, whilst the towing clamp was constrained in every direction other than parallel to the direction of towing. A prescribed displacement was applied to the towing clamp to simulate displacement-controlled deformation. Gravity and thermal effects were neglected. Material properties of the clamps were simulated as linear elastic acrylonitrile butadiene styrene (ABS) plastic, whilst elastic and hyperelastic properties for PDMS were taken from literature (Table 1). The mesh was made of linear quadrilateral elements 1.5 mm in size matched at contact points (Fig. 2a), and mesh convergence was verified. Result were output as strains parallel and perpendicular to the direction of applied displacement (to match experimental results), and surface strains inside the well were measured by averaging across 160 points around the centre of the well after convergence.

**Table 1**

Mechanical properties of PDMS at 1:10 mixing ratio cured at 60 °C for 4 h [25,26].

Linear elastic Material Constant		Hyperelastic (Ogden) Material Constant	
Young's Modulus (MPa)	1.7	$\mu_1$	63.49
Poissons Ratio	0.5	$\mu_2$	0.41
Density (g/cm <sup>3</sup> )	0.97	$\alpha_1$	$6.37 \times 10^{-10}$
		$\alpha_2$	3.81
		Bulk mod. K (MPa)	962

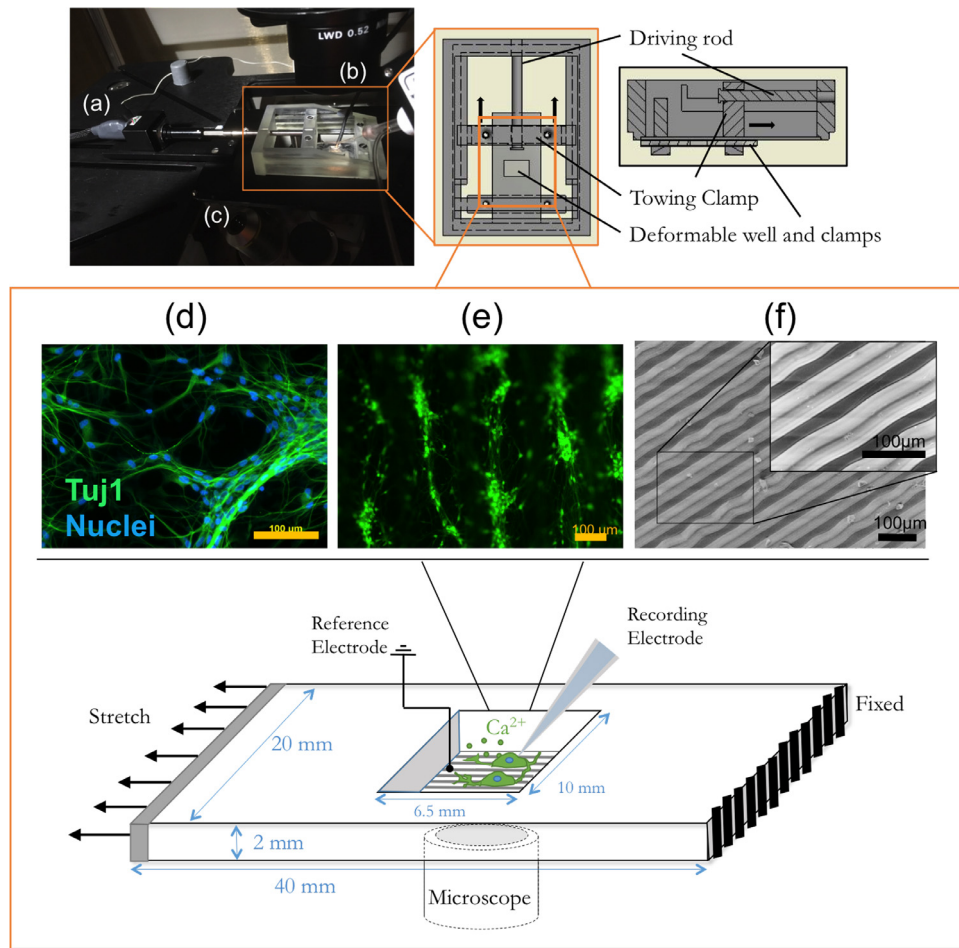


**Fig. 1.** Cell-stretching device setup on Nikon microscope stage adaptor. (a) Linear actuator, controlled from separate controller connected via USB to the controlling PC. (b) Sample holder and clamps. Mounting and unmounting of deformable sample wells can be carried out without removing the device from the microscope stage. (c) Microscope stage adaptor. Magnification: Detail of deformable substrate, showing grooved surface and simultaneous stretch, imaging and electrophysiology. (d–e) iPSC-derived neurons cultured on deformable well substrates extend neurites and form networks. Fluorescent labelling of Tuj1 ( $\beta$ -III tubulin, green) and nuclei (blue) on unpatterned surfaces (d), and on aligned substrates (Tuj1 only) (e). (f) SEM images of aligned grooves. Scale bars = 100  $\mu$ m. (Please refer to the online version of this article to view the figures in color.)

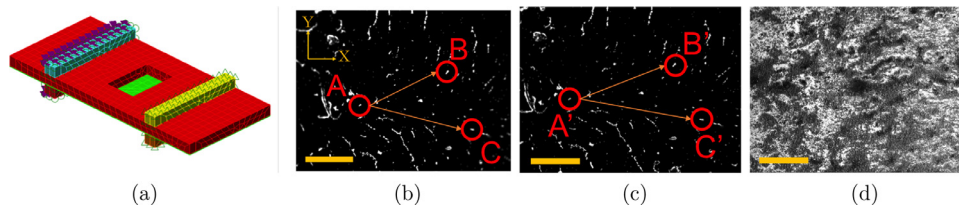


**Fig. 2.** Strain field quantification methods. (a) FE Model showing mesh and constraints. (b–c) Example of bead pattern for strain quantification, before deformation (b) and after 15% prescribed displacement (c). Red arrows show vectors constructed between point triplets. (d) Speckle pattern for digital image correlation quantification. Scale bars = 500  $\mu$ m.

### 2.5. Strain quantification by point tracking

To manually compute surface strains, a 1% solution of 5  $\mu$ m diameter green fluorescent beads (ThermoFisher, 490/520 nm excitation/emission wavelength) in 70% ethanol was applied to the surface of the deformable well and dried under laminar flow. Incremental deformation was applied to deformable wells, and bead patterns were imaged ( $10\times$  lens). Multiple ( $n = 10$  from three independent substrates) triplets of distinct points in the bead pattern were used for analysis (Fig. 2b and 2c) using a Cauchy–Green tensor method, automated using a custom-written MATLAB script [6].

### 2.6. Digital image correlation strain quantification

Digital image correlation (DIC) is a non-invasive method to quantify strains based on surface patterns, and has previously been used to characterise biaxial strain fields applied to substrates and cells [27]. For DIC, surfaces were coated with a 10% solution (v/v) of 1  $\mu$ m diameter polystyrene beads in 70% ethanol (Fig. 2d) to create random patterns, and imaged during deformation ( $4\times$  lens). DIC was performed using GOM Correlate (GOM GmbH), and strains in the X and Y directions were averaged over the entire imaging area (300 points covering  $2.5 \times 1.6$  mm) at the centre of the deformable well.

## 2.7. Cell culture, immunocytochemistry and imaging

Deformable wells were sterilised by immersion in 70% ethanol for 2 h and air dried under sterile laminar flow, followed by exposure to UV light for 15 min. Wells were then treated for 90 s in an Oxygen Plasma Generator (Diener Technologies) to promote cell attachment. Culture surfaces were then coated with 1% matrigel solution (Corning) for 1 h at 37 °C.

Human iPSC-derived motor neurons (iPSCs from StemBANCC, Oxford, UK) differentiated following an established protocol [28] were dissociated using Accutase (ThermoFisher), and seeded at 30,000 cells/well two days prior to stretch experiments. Culture medium was replaced every 24 h. Good cell attachment and extension was observed both on unpatterned and grooved surfaces (Fig. 1(d) and 1(e)).

F11 cells (from ECACC, UK), a rat neuroblastoma and primary dorsal root ganglion neuron hybrid, were chosen as model cells for electrophysiology due to their well characterised action potential firing [29,30]. F11s were seeded at 5000 cells/well and differentiated for five days in high glucose DMEM medium (ThermoFisher) supplemented with 1% foetal bovine serum (ThermoFisher), 1% penicillin/streptomycin (Sigma-Aldrich), 0.5% insulin transferrin selenium (ITS, ThermoFisher), 10  $\mu$ M 3-Isobutyl-1-methylxanthine (IBMX, Sigma-Aldrich), 50 ng/ml nerve growth factor (Peprotech), 2  $\mu$ M all-trans retinoic acid (Sigma-Aldrich) and 0.5 mM bromoadenosine 3',5'-cyclic monophosphate (Sigma-Aldrich).

For immunocytochemistry, cells grown on flat and grooved surfaces were fixed in 3.7% paraformaldehyde (Sigma-Aldrich), permeabilised and blocked in a solution of 0.1% Triton-X, 0.1% Tween-20 and 1% bovine serum albumen (all from Sigma-Aldrich) in phosphate buffered saline (PBS, ThermoFisher). Cells were labelled with chicken anti  $\beta$ -III tubulin primary antibody (Abcam), followed by anti-chicken AlexaFluor488 secondary antibody (ThermoFisher), and nuclei were counterstained with NucBlue (ThermoFisher). Widefield images were taken using an inverted Nikon Ti-E microscope with multi-LED excitation (CoolLED). Confocal images were taken using a Zeiss 710 confocal microscope (63 $\times$  lens, oil immersion).

## 2.8. Stretching procedure

Deformable wells were clamped in place (Fig. 1), and the driving rod was retracted until it contacted the towing clamp. The initial distance between towing and stationary clamp was measured using digital calipers, and this distance was used to calculate displacement and velocity for desired strain (max 70%) and strain rates (set by motor min and max velocities of 0.000893 and 52  $\text{mm s}^{-1}$  respectively). Cells were exposed to strains of 25%, 45% and 70% at a strain rate of 0.1  $\text{s}^{-1}$ .

## 2.9. Quantification of cell morphology changes

To evaluate the effect of substrate strain on cell morphology, membranes and nuclei of live cells were stained by incubating cells for 20 min with 1% CellMask Green and NucBlue (both from ThermoFisher). Nuclei shapes were measured using Ovuscul, an ImageJ plugin (ImageJ, NIH) which fits an ellipse to areas of high contrast and returns major and minor axes measurements [31]. Membrane stretch was measured manually by selecting distinct membrane features and measuring lengths in the same direction as the nucleus major and minor axes. Six independent cell populations on smooth and grooved surfaces were stretched in 10% prescribed displacement increments up to 30%. Cell morphology during deformation was measured for neurons cultured on both aligned groove, and unpatterned surfaces.

## 2.10. Whole-cell patch clamping

The experimental setup for electrophysiological recording consisted of a Digidata 1440A Digitizer and a MultiClamp 700B Amplifier piloted through pCLAMP 10 Software (all from Molecular Devices). Glass micropipettes were pulled to a resistance of 8–10  $\text{M}\Omega$  from thin wall borosilicate tubing (BF100-78-10, Sutter Instruments) using a Flaming/Brown micropipette puller (Model P-1000, Sutter Instruments). Pulling parameters were optimised according to previous work to obtain desired micropipette shape and surface properties [32]. The intracellular solution contained: 140 mM KCl, 5 mM NaCl, 0.5 mM  $\text{CaCl}_2$ , 2 mM  $\text{MgCl}_2$ , 10 mM HEPES, 1 mM GTP and 2 mM ATP, with pH adjusted to 7.4 by addition of KOH and osmolarity adjusted to 300  $\text{mOsm L}^{-1}$  by glucose addition. The bath solution contained: 130 mM NaCl, 5 mM KCl, 2 mM  $\text{CaCl}_2$ , 1 mM  $\text{MgCl}_2$ , 10 mM glucose and 10 mM HEPES, with pH adjusted to 7.4 by addition of NaOH and osmolarity adjusted to 300  $\text{mOsm L}^{-1}$  by glucose addition. To evoke voltage dependent currents, stretched cells were stimulated with a series of depolarising pulses from  $-90$  mV to  $+70$  mV with a step size of 10 mV and currents were recorded in voltage clamp mode. Action potentials were evoked in current clamp mode by a series of current pulses from  $-50$  pA to  $+80$  pA with a step size of 10 pA.

## 2.11. Functional calcium imaging

Calcium activity was imaged using Oregon Green 488 BAPTA-2 calcium indicator [33]. Cells grown on aligned substrates were incubated in a 4  $\mu$ M dye solution in FluoroBrite-DMEM imaging medium (ThermoFisher) for 30 min, washed twice in calcium free PBS, and further incubated in fresh FluoroBrite-DMEM for 30 min. Cells were imaged using standard FITC filters (144/530 nm ex/em) at 10 frames per second for 4 min, and fluorescence intensities from individual cells were recorded over time.

## 2.12. Statistical analysis

Statistical analysis was carried out in PRISM v6 (Graphpad, USA). Data was tested for significance using unpaired T-testing corrected for multiple comparisons by Tukey's test.

# 3. Results

## 3.1. Single cell electrophysiology measurements during strain application

Differentiated F11 cell populations were strained by 45% and whole-cell current and voltage clamp recordings were acquired while the stretch was maintained, to demonstrate the compatibility of our device with simultaneous direct electrophysiology measurements. Inwards (sodium) and outwards (potassium) currents and induced action potentials were recorded from deformed cells (Fig. 3), demonstrating how this system can be used to record neural electrophysiology during acute cell deformation to examine the mechanisms involved in immediate mechanotransduction and primary ion channel and membrane damage.

## 3.2. Functional calcium imaging

Calcium flux imaging of human iPSC-derived neurons on aligned grooved surfaces was acquired for four minutes. Cell activity (Fig. 4) shows that iPSC-derived neurons on grooved deformable substrates mature to form spontaneously active networks which can be imaged using our device. This allows the study of alterations in neural network activity and connectivity under strain. The vertical fluorescence profile from Oregon Green BAPTA-1 stained



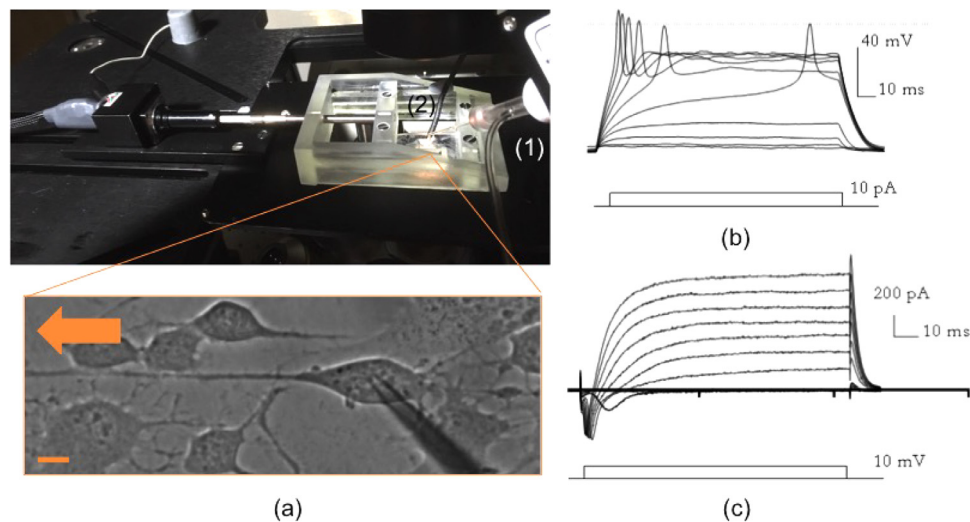


**Fig. 3.** (a) Whole-cell patch clamp setup for recordings from a cell subject to 45% strain. Arrow = direction of alignment and stretch. (1) Shows micromanipulator and recording electrode, (2) shows bath electrode. (b) In current clamp mode, invoked action potentials were recorded. (c) In voltage clamp mode, inwards sodium currents and outwards rectifying potassium currents were recorded. Dotted line = 0 mV. Scale bar = 10  $\mu$ m.

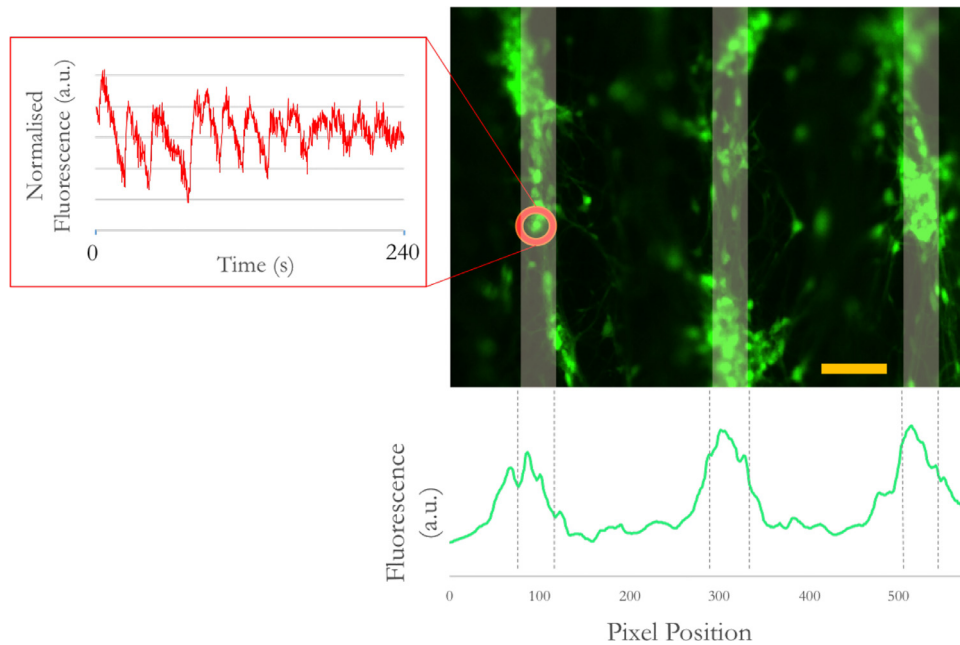


**Fig. 4.** Oregon green BAPTA-1 functional calcium imaging of human iPSC neurons on aligned microgrooved substrates. Surface grooves have been highlighted, and fluorescence intensity profile averaged across the vertical axis plotted (lower graph). Representative calcium signal profile shows spiking activity (left). Scale bar = 100  $\mu$ m.

cells was plotted to show cell clustering within grooves, with distinct peaks corresponding to groove positions (Fig. 4, lower plot). This confirmed cell localisation within substrate features and the formation of aligned bundles of highly polar cells, representative of nerve fibre bundles in peripheral neurons.

### 3.3. Confocal imaging during strain application

Human iPSC-derived neurons were imaged by confocal microscopy ( $63\times$  lens, oil immersion) in both unstrained and 45% strained conditions to reconstruct Z-profiles of cell membranes and nuclei. Cells were imaged in 2  $\mu$ m thick Z-slices, and nucleus heights were reconstructed and measured. Cell nuclei were subjected to induced vertical compression and nucleus height decreased by 10% when stretch was applied (Fig. 5).

### 3.4. Experimental and simulated substrate strain characterisation

The mechanical properties of the deformable wells were characterised by simulated surface strain as a result of applied grip-to-grip strain, validated by experimental measurements. Experimental and simulated strains all showed strong linear correlations with applied grip-to-grip strain (Fig. 6a, average  $R^2 > 0.97$ ). Simulated and experimental values of strains parallel ( $E_{xx}$ ) and perpendicular ( $E_{yy}$ ) to the applied deformation were strongly correlated, indicating that the simulations robustly predicted system mechanical properties. The best fit was achieved by using Ogden hyperelastic PDMS properties (Table 1), as previously reported [25,34]. Average slope values for hyperelastic simulated and experimental data were  $2.325 (\pm 0.02)$  and  $0.501 (\pm 0.05)$  for  $E_{xx}$  and  $E_{yy}$ , respectively.  $E_{xx}$  to  $E_{yy}$  ratio increased linearly with applied strain ( $R^2 > 0.99$ ),

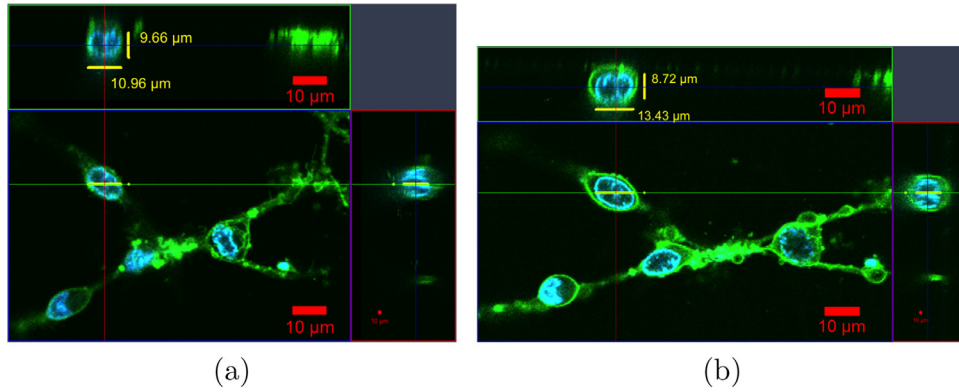


**Fig. 5.** High-resolution z-slice imaging of iPSC-derived neuron nuclei and membranes during strain application. Volume reconstructions shows how cell nuclei are compressed as a result of substrate deformation. Confocal z-slice imaging of cells stained for membrane and nuclei is used to measure nucleus height before (a) and after (b) a 45% substrate deformation. Yellow line shows measurement of nucleus height. Scale bar = 10  $\mu\text{m}$ . (Please refer to the online version of this article to view the figures in color.)

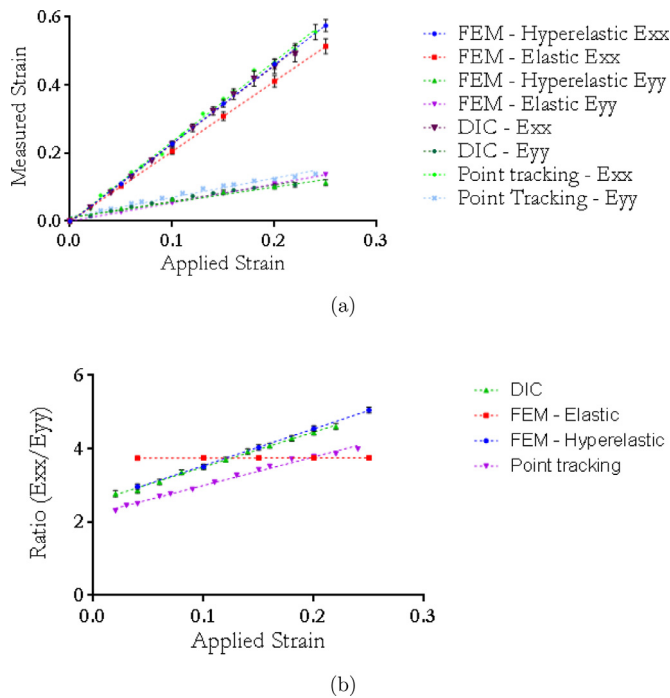


**Fig. 6.** (a) Absolute measured experimental strains parallel ( $E_{xx}$ ) and perpendicular ( $E_{yy}$ ) to applied deformation, for experimental and simulated data. (b) Ratio of parallel ( $E_{xx}$ ) to perpendicular ( $E_{yy}$ ) strain for increasing applied (grip-to-grip) strain, for experimental and simulated data.

except in elastic material model simulations, for which the ratio was constant (Fig. 6b).

### 3.5. Surface Strain of microgrooved substrates

Microgroove topography was characterised by SEM imaging (Fig. 1(f)). The average groove width was  $50 \pm 1.7 \mu\text{m}$  ( $n = 30$ , from three independently cast samples), the groove depth was estimated to be  $20 \mu\text{m}$ , and the alignment was measured at  $0.53^\circ$ , characterised by the standard deviation of groove angle with respect to the horizontal. With the selected well geometry, the strain field at the centre of the substrate was found to be uniform for both smooth and patterned surfaces (Fig. 7 a and b). Strain simulations showed that the presence of microgrooves did not affect the average mechanical behaviour of the deformable wells (Fig. 7 c and d). The experimental calibration curve derived from DIC and

point tracking (Fig. 6a) can therefore also be used for grooved surfaces. These results show how a grooved substrate, which promotes cell growth along the axis of deformation, can be combined with uniaxial stretch to more realistically model peripheral neuron deformation.

### 3.6. Cell deformation in aligned microgrooves

Nuclei and membranes were measured during strain to evaluate the effect of grooved substrates on the change in cell shape (Fig. 8a). On unpatterned substrates, cell response was heterogeneous with a large range of positive and negative strains recorded along the cell major axes. Patterned, grooved substrates induced cell and neurite alignment along the surface topography (Fig. 1) and resulted in higher average nucleus and membrane strains and lower standard deviation (Fig. 8c, 8b).

Another measure of cellular deformation is strain transfer between cell components, termed the strain partitioning ratio (SPR) [35]. The cell membrane, adhering through focal adhesions to the substrate, deforms as a result of applied displacement and the cytoskeleton transfers a proportion of strain to the nucleus [36]. Comparing cells stretched on aligned grooves and unpatterned substrates, the SPR increased significantly with alignment for both membranes and nuclei and did not vary significantly with increased deformation (Fig. 8d and 8e). Average substrate-nucleus SPR was 30% in aligned cells, and 15% in cells cultured on unpatterned substrates. Average substrate-membrane SPR was 65% in aligned cells, and 50% in cells cultured on unpatterned substrates.

## 4. Discussion

### 4.1. Electrophysiological measurements and imaging during cell straining

Understanding multi-scale PNS mechanics can help to identify mechanisms of conduction blocks as well as sensory and motor function alteration due to trauma. Existing cell-stretching devices do not allow simultaneous cell deformation and electrophysiological recording [2,3,37,38], and so it is not possible to capture ion currents and action potentials in the stretched state. Flexible MEA-based devices allow for measurement of spontaneous electrophysiological activity of neurons subject to shear in cultured cells [13], as well as strain in hippocampal tissue slices and sciatic nerves [14,15], but are limited in compatibility with imaging setups and do not provide data about ion channel functionality,

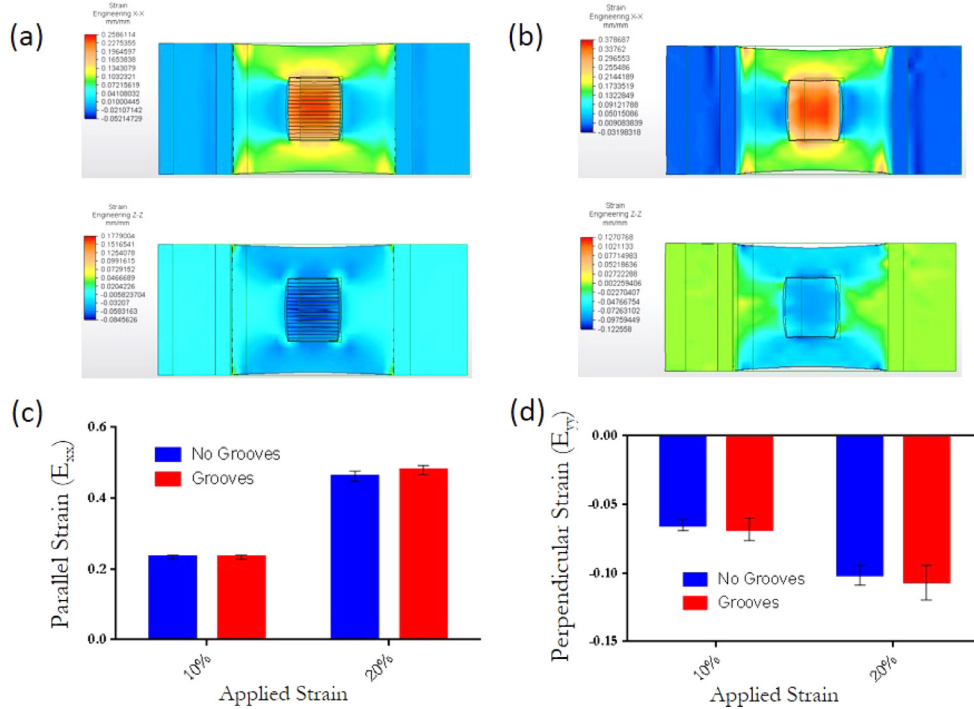


**Fig. 7.** Simulation results show that grooves do not significantly affect substrate strains. (a) Axial strain is not significantly altered by grooves, neither is longitudinal strain (b). Strain heat maps for grooved (c) and smooth (d) surfaces show uniform strain distribution around centre of well.

which is known to play a key role in the electrophysiological response to strain [2,3].

Our results show how we can acquire both single-cell and network electrophysiology measurements from cells in a stretched state. In previous studies, simultaneous single-cell electrophysiology and direct mechanical perturbation has been achieved by micro-indentation [39], by fluid streaming onto the cell [40], and by localised membrane suction [2]. These methods locally strain a small area of the membrane and do not represent physiological deformation conditions. The design of our device allows uniform whole-cell deformation to be transferred from substrate to cells during electrophysiological measurements.

Another key system feature is its compatibility with multiple imaging setups, as most existing designs do not allow high resolution imaging during stretch [41]. Our device can be mounted on an inverted or upright microscope stage, and the ultra-thin deformable substrates are compatible with high magnification lens imaging, allowing reconstructions of Z-stacks for 3D imaging. The ability to measure nucleus height before and during straining (Fig. 5) highlights the suitability of this stretching device for use in conjunction with high-resolution imaging during *in situ* cell deformation. This technique can be applied to investigate the effect of cytoskeletal manipulation on cell mechanics.

#### 4.2. Strain characterisation

Simulation results for resulting local strain at the deformable well surface were validated by experimental measurements (Fig. 6a). Finite element method simulations were used to design the well, such that the strain field generated at the surface of the culture substrate was uniform around the centre. This was achieved by optimising the well shape and size (data not shown). The size of the well was optimised to reduce reagent waste, while containing enough medium to avoid rapid evaporation, previously highlighted as key design parameters [5].

Strain results were used to construct a calibration curve, relating the applied grip-to-grip strain to the local surface strain. A linear ratio of  $2.325 (\pm 0.02)$  and  $0.501 (\pm 0.05)$  for  $E_{xx}$  and  $E_{yy}$  was found, representing the factors by which grip-to-grip strain is transferred to the cell culture surface.

A key property of the system is the ratio of  $E_{xx}$  to  $E_{yy}$ . Biomechanical studies on peripheral nerve have shown a unique Poisson behaviour with nerves compressing radially during axial elongation [20], which has not been reported in an *in vitro* model. The ratio of  $E_{xx}$  to  $E_{yy}$  increased with grip-to-grip strain, and experimental measurements validated hyperelastic simulation results (Fig. 6b), confirming that PDMS can be better described to have hyperelastic properties, and indicating that the non-constant ratio observed can be explained by material properties instead of grip slipping.

#### 4.3. Microgrooved surface characterisation

Deformable substrate surfaces were patterned with aligned microgrooves, which induce cells to grow parallel to the direction of applied strain. Bipolar cells such as neurons have cytoskeletons aligned with cell polarity [42], which allows more deformation in cells parallel to applied substrate deformation. This results in anisotropic cell deformation, which has been shown to translate from the cytoskeleton to the nucleus [36,43]. Deformation is therefore more reproducible and uniform, which is more representative of the physiological conditions in peripheral nerves where neural fibres are aligned axially and therefore exposed to strains aligned with fibre polarity.

Our results show that aligning cells by embedded substrate topography reduces the variability of deformation, more closely resembling *in vivo* peripheral nerve conditions, whilst maintaining accessibility for electrophysiology and access for inverted microscopy. The presence of substrate grooves also provides physical support to cells, more closely replicating the mechanical environment of peripheral nerve.

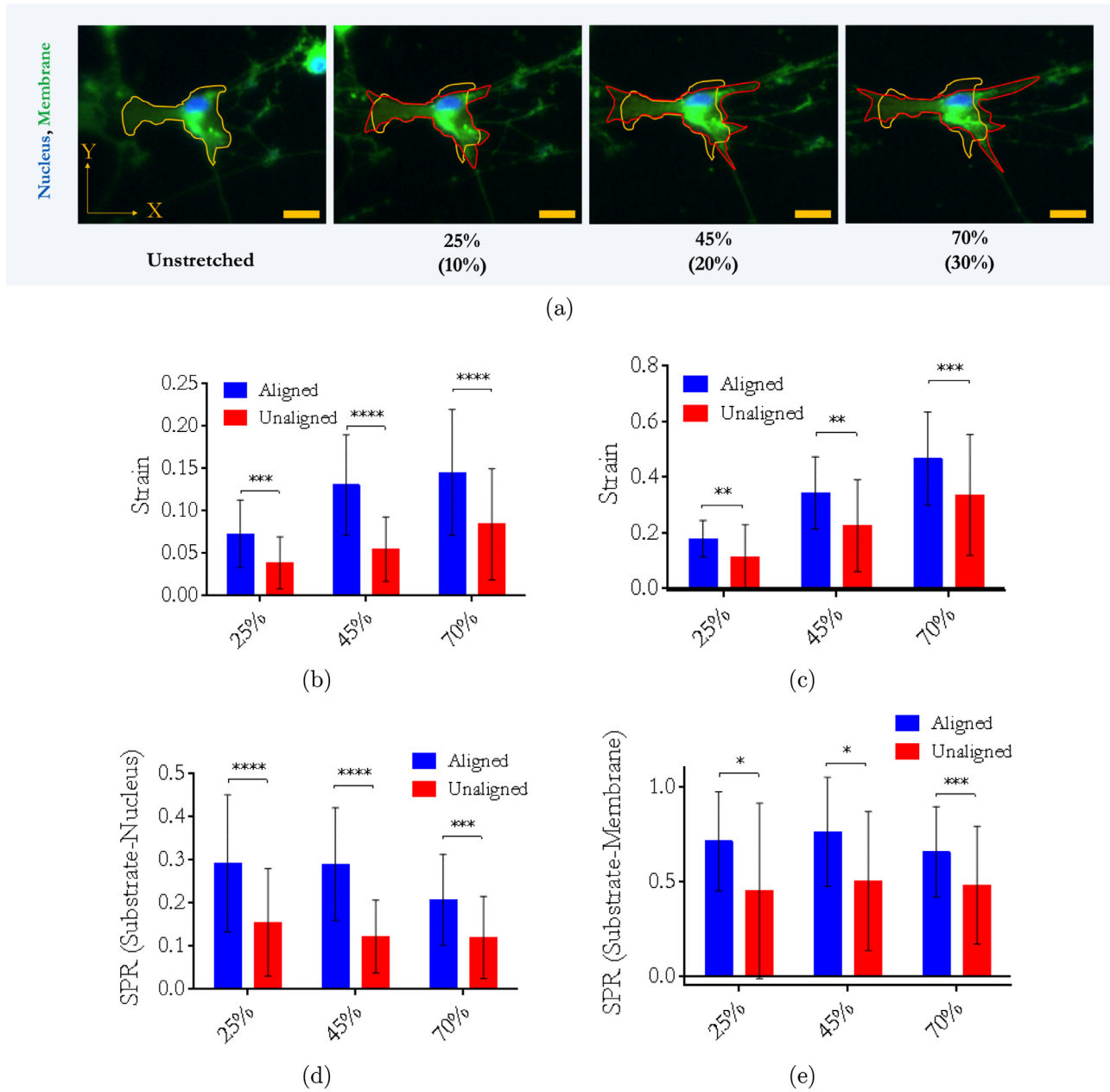


**Fig. 8.** (a) Incremental cell deformation (nuclei stained with NucBlue and membrane stained with CellMask green). Strain values in brackets represent applied grip-to-grip strain (along x-axis). Scale bar = 10  $\mu\text{m}$ . Yellow outline shows initial cell shape (at 0% strain). Red outline shows deformed cell at each strain. Nucleus (b) and membrane (c) average strain is significantly higher for cells cultured on parallel groove surfaces, compared to unpatterned surfaces. Nucleus (d) and membrane (e) SPR is significantly higher, on average, for cells cultured on parallel groove surfaces, compared to unpatterned surfaces. X-axis values show applied grip-to-grip strain. Bars show mean  $\pm$  S.D. \*\*\*\* =  $p < 0.0001$ , \*\*\* =  $p < 0.001$ , \*\* =  $p < 0.01$ , \* =  $p < 0.05$ .  $n > 25$  for all measurements. (Please refer to the online version of this article to view the figures in color.)

Compartmentalised microfluidic devices have been previously used to induce alignment and study injury applied by a localised pressure pulse [24]. This requires cells to be fully enclosed, precluding direct access for electrophysiology. Furthermore, localised injury is less representative of peripheral nerve trauma, compared to whole-cell stretch. Pressure-pulse systems, developed to investigate the effect of stretch on axons [9] and subsequently used in numerous studies [23,44,45] have also been used with growth templates to align axons [46]. However, the pressure-pulse design requires an enclosed pressure chamber, again precluding access to cells for direct electrophysiology. Growth template masks have also been used to align neurons during culture before applying uniaxial stretch [7], but they do not provide physical support and can damage cultures when removed. By patterning the cell

culture substrate, we can induce cell alignment without risking cell damage, while allowing direct access to cells for electrophysiological measurements.

## 5. Conclusions and limitations

Research into the effects of mechanical strain on the PNS has implications in trauma prevention, recovery and regeneration. To better understand the effects of macro-scale deformation on individual neurons, *in vitro* models replicating the mechanical environment of peripheral nerve tissue are required.

Cell-substrate stretching devices have been used extensively to model TBI and to study the effect of uniaxial [6,7,9] and biaxial [14,47,48] strain, but no system allows direct single-cell



electrophysiological measurements of deformed neurons within an environment which emulates PNS tissue morphology coupled with high resolution microscopy.

We present and characterise a novel substrate-stretching device which can be used to apply axial strains at a large range of strain rates to populations of neurons grown on ultra-thin deformable substrates, both smooth and patterned with aligned grooves. The mechanical behaviour of unpatterned and grooved deformable culture surfaces was characterised experimentally and numerically to precisely calibrate cell strains. We show compatibility with high-magnification imaging, single-cell and network electrophysiology recordings of cells during the application of strain, indicating how the device can be used as a platform for an experimental multi-physics investigation of the effect of stretch on peripheral neurons.

Overall, the device presented provides a compact, flexible, and adaptable tool for peripheral nerve mechanobiology and electro-mechanical studies. The thorough characterisation describes a repeatable *in vitro* model for the study of the effect of stretch on peripheral neurons. It is hoped that use of such models will lead to a better understanding of the causes of traumatic neuropathy, as well as the optimisation of strategies for damage prevention and repair.

Some limitations still need to be overcome. For instance, myelination of PNS axons is known to play a role in the response to mechanical damage [49]. Integrating aligned Schwann cell-neuron cocultures would increase the physiological relevance of the model and allow studies of regeneration following mechanical trauma. The compartmentalisation of neural cell bodies and axons to different regions within the model would also increase the similarity between PNS tissue and the model. The current design of the device relies solely on displacement control. To overcome this, force control could be implemented, and parameters matched to experimentally obtained properties of nerve tissue during tensile testing. A limitation of the current design of the device is that cells are not kept in a temperature controlled, sterile, or humidified environment during stretching. This, together with medium evaporation from the open stretch chamber makes the current device unsuitable for long-term experiments.

## Acknowledgements

Authors acknowledge China Regenerative Medicine Limited (CRMI) for funding and the EPSRC DTP award number 1514540 for F.B. funding. M.B. and A.J. acknowledge funding from the European Union's Seventh Framework Programme (FP7 20072013) ERC Grant agreement no. 306587. The authors would like to thank Mr. James (Jim) Fisk and Mr. David Salisbury for their assistance with manufacturing, Mr. Graham Brown for help with confocal microscopy, Dr. Kalin Dragnevski for help with SEM operation and Ms. Linda Li for early work on the device. The authors declare no conflict of interests. No ethical approval was required.

## Supplementary material

Supplementary material associated with this article can be found in the online version at doi:10.1016/j.medengphy.2019.02.014.

## References

- [1] Gilbert WM, Nesbitt TS, Danielsen B. Associated factors in 1611 cases of brachial plexus injury. *Obstet Gynecol* 1999;93(4):536–40.
- [2] Wang JA, Lin W, Morris T, Banderli U, Juranka PF, Morris CE. Membrane trauma and na<sup>+</sup> leak from nav1.6 channels. *Am J Physiol Cell Physiol* 2009;297(4):C823–34.
- [3] Goforth PB, Ren J, Schwartz BS, Satin LS. Excitatory synaptic transmission and network activity are depressed following mechanical injury in cortical neurons. *J Neurophysiol* 2011;105(5):2350–63.
- [4] Yap YC, King AE, Guijt RM, Jiang T, Blizzard CA, Breadmore MC, et al. Mild and repetitive very mild axonal stretch injury triggers cytoskeletal mislocalization and growth cone collapse. *PLoS One* 2017;12(5):e0176997.
- [5] Kamble H, Barton MJ, Jun M, Park S, Nguyen N-T. Cell stretching devices as research tools: engineering and biological considerations. *Lab Chip* 2016;16(17):3193–203.
- [6] Pfister BJ, Weihs TP, Betenbaugh M, Bao G. An *in vitro* uniaxial stretch model for axonal injury. *Ann Biomed Eng* 2003;31(5):589–98.
- [7] Nakadate H, Fukumura Y, Kaneko Y, Kakuta A, Furukawa H, Aomura S. *In vitro* uniaxial stretch model for evaluating the effect of strain along axon on damage to neurons. *J Biomech Sci Eng* 2014;9(3):14–00136.
- [8] Geddes DM, Cargill 2nd RS, LaPlaca MC. Mechanical stretch to neurons results in a strain rate and magnitude-dependent increase in plasma membrane permeability. *J Neurotrauma* 2003;20(10):1039–49.
- [9] Smith DH, Wolf JA, Lusardi TA, Lee VM, Meaney DF. High tolerance and delayed elastic response of cultured axons to dynamic stretch injury. *J Neurosci* 1999;19(11):4263–9.
- [10] LaPlaca MC, Thibault LE. An *in vitro* traumatic injury model to examine the response of neurons to a hydrodynamically-induced deformation. *Ann Biomed Eng* 1997;25(4):665–77.
- [11] Kamotani Y, Bersano-Begey T, Kato N, Tung Y-C, Huh D, Song JW, et al. Individually programmable cell stretching microfluidic arrays actuated by a braille display. *Biomaterials* 2008;29(17):2646–55.
- [12] Iwade Y, Yumura S. Cyclic stretch of the substratum using a shape-memory alloy induces directional migration in dictyostelium cells. *Biotechniques* 2009;47(3):757–67.
- [13] Prado GR, Ross JD, DeWeerth SP, LaPlaca MC. Mechanical trauma induces immediate changes in neuronal network activity. *J Neural Eng* 2005;2(4):148–58.
- [14] Lacour SP, Benmerah S, Tarte E, FitzGerald J, Serra J, McMahon S, et al. Flexible and stretchable micro-electrodes for *in vitro* and *in vivo* neural interfaces. *Med Biol Eng Comput* 2010;48(10):945–54.
- [15] Kang WH, Cao W, Graudejus O, Patel TP, Wagner S, Meaney DF, et al. Alterations in hippocampal network activity after *in vitro* traumatic brain injury. *J Neurotrauma* 2015;32(13):1011–19.
- [16] Loverde JR, Pfister BJ. Developmental axon stretch stimulates neuron growth while maintaining normal electrical activity, intracellular calcium flux, and somatic morphology. *Front Cell Neurosci* 2015;9:308.
- [17] Bhattacharya MRC, Bautista DM, Wu K, Haeberle H, Lumpkin EA, Julius D. Radial stretch reveals distinct populations of mechanosensitive mammalian somatosensory neurons. *Proc Natl Acad Sci U S A* 2008;105(50):20015–20.
- [18] Higgins S, Lee JS, Ha L, Lim JY. Inducing neurite outgrowth by mechanical cell stretch. *Biores Open Access* 2013;2:212–16.
- [19] Shibasaki K, Murayama N, Ono K, Ishizaki Y, Tominaga M. TRPV2 enhances axon outgrowth through its activation by membrane stretch in developing sensory and motor neurons. *J Neurosci* 2010;30(13):4601–12.
- [20] Topp KS, Boyd BS. Structure and biomechanics of peripheral nerves: nerve responses to physical stresses and implications for physical therapist practice. *Phys Ther* 2006;86(1):92–109.
- [21] Kobayashi S, Shizu N, Suzuki Y, Asai T, Yoshizawa H. Changes in nerve root motion and intradiscal blood flow during an intraoperative straight-leg-raising test. *Spine* 2003;28(13):1427–34.
- [22] Weiss P. Experiments on cell and axon orientation *in vitro*; the role of colloidal exudates in tissue organization. *J Exp Zool* 1945;100:353–86.
- [23] Tang-Schomer MD, Patel AR, Baas PW, Smith DH. Mechanical breaking of microtubules in axons during dynamic stretch injury underlies delayed elasticity, microtubule disassembly, and axon degeneration. *FASEB J* 2010;24(5):1401–10.
- [24] Yap YC, Dickson TC, King AE, Breadmore MC, Guijt RM. Microfluidic culture platform for studying neuronal response to mild to very mild axonal stretch injury. *Biomicrofluidics* 2014;8(4):044110.
- [25] Kim TK, Kim JK, Jeong OC. Measurement of nonlinear mechanical properties of PDMS elastomer. *Microelectron Eng* 2011;88(8):1982–5.
- [26] Johnston ID, McCluskey DK, Tan C, others. Mechanical characterization of bulk sylgard 184 for microfluidics and microengineering. *J Micromech Microeng* 2014.
- [27] Bieler FH, Ott CE, Thompson MS, Seidel R, Ahrens S, Epari DR, et al. Biaxial cell stimulation: a mechanical validation. *J Biomech* 2009;42(11):1692–6.
- [28] Bianchi F, Malboubi M, Li Y, George JH, Jerusalem A, Szele F, et al. Rapid and efficient differentiation of functional motor neurons from human iPSC for neural injury modelling. *Stem Cell Res* 2018;32:126–34.
- [29] Fan SF, Shen KF, Scheidegger MA, Crain A SM. FII neuroblastoma × DRG neuron hybrid cells express inhibitory/I- and 6-opioid receptors which increase voltage-dependent K<sup>+</sup> currents upon activation. *Brain Res* 1992;590:329–33.
- [30] Kusano K, Gainer H. Modulation of voltage-activated Ca currents by pain-inducing agents in a dorsal root ganglion neuronal line, F-11. *J Neurosci Res* 1993;34(2):158–69.
- [31] Thévenaz P, Delgado-Gonzalo R, Unser M. The ovuscul. *IEEE Trans Pattern Anal Mach Intell* 2011;33(2):382–93.
- [32] Malboubi M, Gu Y, Jiang K. Characterization of surface properties of glass micropipettes using SEM stereoscopic technique. *Microelectron Eng* 2011;88(8):2666–70.
- [33] Grienberger C, Konnerth A. Imaging calcium in neurons. *Neuron* 2012;73(5):862–85.
- [34] Brandrup J, Immergut EH, Grulke EA, Abe A, Bloch DR. Polymer handbook, 7. Wiley, New York etc; 1989.

- [35] Gilchrist CL, Witvoet-Braam SW, Guilak F, Setton LA. Measurement of intracellular strain on deformable substrates with texture correlation. *J Biomech* 2007;40(4):786–94.
- [36] Tremblay D, Andrzejewski L, Leclerc A, Pelling AE. Actin and microtubules play distinct roles in governing the anisotropic deformation of cell nuclei in response to substrate strain. *Cytoskeleton* 2013;70(12):837–48.
- [37] Magou GC, Pfister BJ, Berlin JR. Effect of acute stretch injury on action potential and network activity of rat neocortical neurons in culture. *Brain Res* 2015;1624(Supplement C):525–35.
- [38] Tavalin SJ, Ellis EF, Satin LS. Mechanical perturbation of cultured cortical neurons reveals a stretch-induced delayed depolarization. *J Neurophysiol* 1995;74(6):2767–73.
- [39] Drew LJ, Wood JN. FM1-43 is a permeant blocker of mechanosensitive ion channels in sensory neurons and inhibits behavioural responses to mechanical stimuli. *Mol Pain* 2007;3:1.
- [40] McCarter GC, Reichling DB, Levine JD. Mechanical transduction by rat dorsal root ganglion neurons *in vitro*. *Neurosci Lett* 1999;273(3):179–82.
- [41] Nguyen B-NB, Chetta J, Shah SB. A novel technology for simultaneous tensile loading and High-Resolution imaging of cells. *Cell Mol Bioeng* 2012;5(4):504–13.
- [42] Khatau SB, Hale CM, Stewart-Hutchinson PJ, Patel MS, Stewart CL, Searson PC, et al. A perinuclear actin cap regulates nuclear shape. *Proc Natl Acad Sci U S A* 2009;106(45):19017–22.
- [43] Haase K, Macadangdang JKL, Edrington CH, Cuerrier CM, Hadjiantoniou S, Harden JL, et al. Extracellular forces cause the nucleus to deform in a highly controlled anisotropic manner. *Sci Rep* 2016;6:21300.
- [44] Iwata A, Stys PK, Wolf JA, Chen X-H, Taylor AG, Meaney DF, et al. Traumatic axonal injury induces proteolytic cleavage of the voltage-gated sodium channels modulated by tetrodotoxin and protease inhibitors. *J Neurosci* 2004;24(19):4605–13.
- [45] Wolf JA, Stys PK, Lusardi T, Meaney D, Smith DH. Traumatic axonal injury induces calcium influx modulated by tetrodotoxin-sensitive sodium channels. *J Neurosci* 2001;21(6):1923–30.
- [46] Tang-Schomer MD, Johnson VE, Baas PW, Stewart W, Smith DH. Partial interruption of axonal transport due to microtubule breakage accounts for the formation of periodic varicosities after traumatic axonal injury. *Exp Neurol* 2012;233(1):364–72.
- [47] Geddes DM, Cargill 2nd RS. An in vitro model of neural trauma: device characterization and calcium response to mechanical stretch. *J Biomech Eng* 2001;123(3):247–55.
- [48] Lacour SP, Tsay C, Wagner S, Yu Z, Morrison B. Stretchable micro-electrode arrays for dynamic neuronal recording of in vitro mechanically injured brain. In: *Proceedings of the IEEE Sensors*; 2005. 2005, 4.
- [49] Shreiber DI, Hao H, Elias RAL. Probing the influence of myelin and glia on the tensile properties of the spinal cord. *Biomech Model Mechanobiol* 2009;8(4):311–21.